Analysis and Design of a Digital-Controlled Single-Stage Series-Type LED Driver With Independent N-Channel Output Currents

Jian Huang, Quanming Luo, *Member, IEEE*, Qingqing He, Aqian Zu, and Luowei Zhou, *Senior Member, IEEE*

***Abstract*—In the applications such as mixed-color light emitting diode (LED) lighting system, LED drivers are always required to provide constant current for each LED string and each current should be controlled independently. For this purpose, a single-stage series-type LED driver with independent control of N-channel output currents is proposed in this paper. The function of power factor correction can be realized inherently to obtain high power factor. N active output units, each one made up of a power switch, a diode, and an output filter capacitor, are series-connected to form the series-type N-channel outputs structure. According to different current reference values, N-channel output currents can be independently regulated just by sampling each output current to adjust the duty cycle of each secondary output-switch automatically. The operating principle and independent closed-loop control strategy of the proposed LED driver with $N = 3$ are analyzed as an example in detail. Finally, the quantitative parameter design method for a 120 W prototype is elaborated. And, the experimental results are presented to verify the effectiveness of the LED driver and the correctness of parameter design method.**

***Index Terms*—Active output unit (AOU), independent control of current, light emitting diode (LED) driver, N-channel outputs.**

I. Introduction

LIGHT emitting diode (LED), as a new kind of green lighting source, which uses solid semiconductor chip as luminescent material to convert electric energy into light energy directly, has many outstanding advantages such as long lifetime, high lighting efficiency and non-pollution, etc. Therefore, LEDs have been widely used in lighting field [1]–[4]. In the applications of mixed-color LED lighting, for instance, multi-color LED ambient lighting system, RGB mixed-color LED lamp, LED projection, LED driver with multiple output currents are required to drive multiple LED strings. Moreover, each output current always needs to be controlled independently [5]–[7].

To achieve independent control of multiple output currents, the most direct way is to add a current regulator for each LED

Manuscript received April 18, 2018; revised July 9, 2018 and October 7, 2018; accepted December 4, 2018. Date of publication December 14, 2018; date of current version June 10, 2019. This work was supported by the National Nature Science Foundation of China under Grant 51577019. Recommended for publication by Associate Editor L. Huber. *(Corresponding author: Jian Huang.)*

The authors are with the State Key Laboratory of Power Transmission Equipment and System Security and New Technology, Chongqing University, Chongqing 400044, China (e-mail:

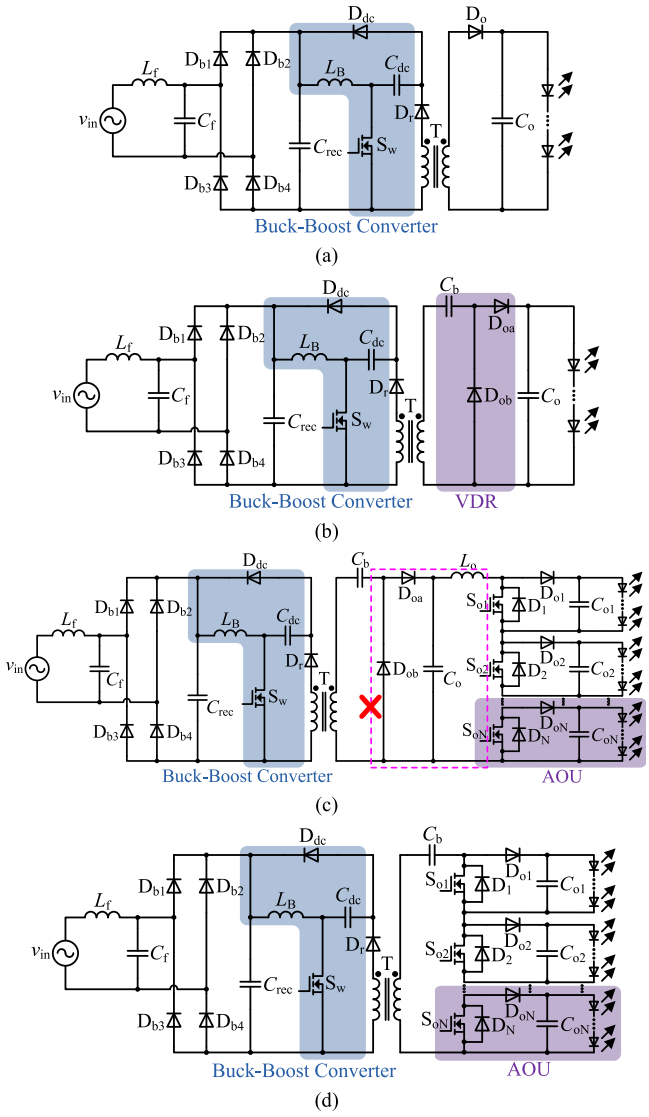

Fig. 1. Topology derivation of the proposed LED driver with independent control of N-channel output currents.

output currents can be realized by adopting different ON–OFF control for all power switches. Accordingly, a single-inductor LED driver for N series-connected LED channels has been introduced in [19], which has the merits of 1) just requiring N switches, 2) allowing concurrent driving of all LED channels in every switching period, and 3) being insensitive to the transition switching from one channel to another. However, the input of this LED driver is dc voltage, which will limit its utilization in ac input applications.

In [20], a single-stage isolated high power factor LED driver with leakage inductor energy recycling is proposed as shown in Fig. 1(a), which integrates a Buck–Boost converter with a Flyback converter by sharing a power switch. The Buck–Boost converter operating in DCM can achieve high power factor internally. The voltage spike and ringing on the power switch is alleviated due to the leakage inductor energy is recycled via a unidirectional diode, so the switching loss can be reduced. However, lower magnetic core utilization results in large volume of the transformer and limits its use in high power applications. To improve the magnetic core utilization and increase the power level, a voltage doubler rectifier (VDR) is added in the secondary side of the transformer as shown in Fig. 1(b), thus, the energy can be transferred whenever the switch is turned ON or turned OFF. Furthermore, the voltage stress of the secondary diodes can be reduced remarkably to lower the switching loss [21]. Due to the advantages of the single-inductor series-type LED driver presented in [19], the N series-connected LED channels can be used to achieve independent control of each output current. That is to say, the single inductor with N series-connected LED channels can be directly regarded as the load of the LED driver with VDR, as shown in Fig. 1(c), where each LED channel has been added a parallel-connected output filter capacitor compared with the LED driver in [19]. It can ensure that the LED channels can be activated at full power and the high-frequency ripple of output currents can be filtered to obtain smooth output currents. According to the ampere-second balance principle, the current flows through the inductor $L_{\rm o}$ is equal to the discharge current of the secondary blocking capacitor $C_{\rm b}$. For the sake of simplifying the topology structure and saving the cost, two output diodes $D_{\rm oa}/D_{\rm ob}$, a filter capacitor $C_{\rm o}$, and a single inductor $L_{\rm o}$ all can be removed. Therefore, a single-stage series-type LED driver with independent N-channel output currents can be proposed as depicted in Fig. 1(d). The secondary blocking capacitor is employed to ensure the volt-second balance of transformer and then provide the common input current of all LED channels after the primary switch is turned OFF. Here, a parallel-connected power switch, an output diode, and an output filter capacitor can be regarded as an active output unit (AOU). All AOUs are series-connected to form the series-type N-channel outputs structure, which can be driven concurrently in a switching period. By regulating the duty cycles of all output-switches $S_{\rm o1}$–$S_{\rm oN}$ can make sure that the conduction time of each AOU is not equal. Hence, independent control of N-channel output currents can be achieved easily.

In the following sections, the proposed LED driver with $N = 3$ has been theoretically analyzed and experimentally validated in detail. The main contents of this paper is organized as follows. In Section II, the operating principle of LED driver is described. The independent closed-loop control strategy (ICCS) in digital signal processor (DSP) and the quantitative parameter design method are presented in detail in Sections III and IV, respectively. The experimental results are given in Section V, and a detailed comparative analysis is made in Section VI. Finally, the conclusions are summarized in Section VII.

II. Analysis of Operating Principle

A. Circuit Description

The equivalent circuit of the proposed LED driver with $N = 3$ is depicted in Fig. 2, where the ac input voltage source, the LC low-pass filter, and the diode bridge rectifier are substituted by a rectified sinusoidal voltage source $V_{\rm rec}$ and a series-connected diode $D_{\rm rec}$. Besides, the isolation transformer T is modeled by an ideal transformer with a parallel-connected magnetizing

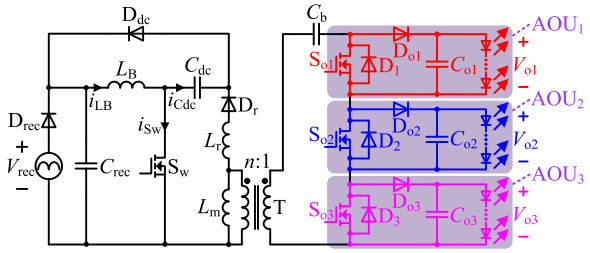

Fig. 2. Equivalent circuit of the proposed LED driver with $N = 3$.

inductor L_m and a series-connected leakage inductor L_r, where the turns ratio is defined as n.

The Buck–Boost PFC unit is formed with a power switch S_w, a diode D_{dc}, an inductor L_B, and an energy-stored capacitor C_{dc}, whose main function is to obtain high input power factor. Besides, the isolated series-type three-channel outputs dc/dc conversion unit is formed with the same power switch S_w and capacitor C_{dc}, a diode D_r, an isolation transformer T, a blocking capacitor C_b, and three AOU (that is AOU_1, AOU_2, and AOU_3), whose main function is to realize electrical isolation and fully independent regulation of each output current. It can be seen that the structures of three AOUs are same and each of them is made up of an output switch, an output diode, and an output filter capacitor, where D_1, D_2, and D_3 are the intrinsic diodes of S_{o1}, S_{o2}, and S_{o3}, respectively. Additionally, the snubber capacitor C_{rec} is used to recycle the leakage energy of the isolation transformer.

B. Operating Mode Analysis

Here, assume that the average values of three output currents to satisfy the following relationship: $I_{o3} > I_{o2} > I_{o1}$. The analysis processes are nearly similar when the relationship among the values of I_{o1}, I_{o2}, and I_{o3} is changed. Since the inductor current i_{LB} and the magnetizing inductor current i_{Lm} are both designed to operate in DCM, there are a total of nine operating modes during an entire switching period T_s. The main operating waveforms and the equivalent circuits for each operating mode are shown in Figs. 3 and 4, respectively. As shown in Fig. 3, i_{LB} is supposed to decrease from peak value to zero earlier than i_{Lm}, and Q_w, Q_1, Q_2, and Q_3 denote the drive signals of four switches S_w, S_{o1}, S_{o2}, and S_{o3}, respectively.

Mode I [t_0–t_1, Fig. 4(a)]: The primary switch S_w is in ON-state, while the switches S_{o1}, S_{o2}, and S_{o3} are in OFF-state. The inductor current i_{LB} increases linearly from zero at time t_0 and the energy-stored capacitor C_{dc} begins to discharge. Besides, the magnetizing inductor current i_{Lm} and the leakage inductor current i_{Lr} also increase linearly from zero as the magnetizing inductor L_m is clamped by the voltage nV_{Cb} in this mode. However, i_{Lr} increases faster than i_{Lm} as the value of the leakage inductor L_r is much smaller than that of the magnetizing inductor L_m, so that the secondary side blocking capacitor C_b begins to charge and the three output filter capacitors C_{o1}, C_{o2}, and C_{o3} release energy to supply respective LED string. At time t_1, S_{o1}, S_{o2}, and S_{o3} are both turned ON under zero voltage condition and the driver goes into the next mode.

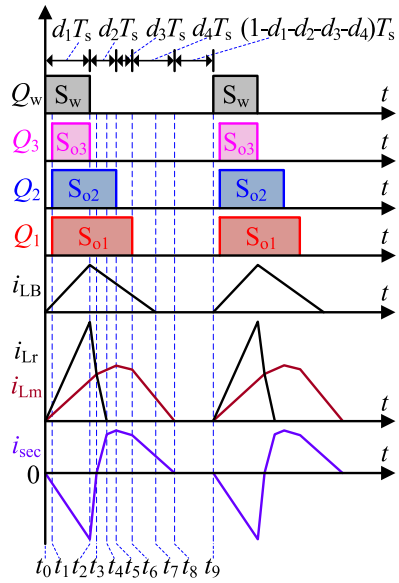

Fig. 3. Main operating waveforms.

Mode II [t_1–t_2, Fig. 4(b)]: The switches S_w, S_{o1}, S_{o2}, and S_{o3} are all in ON-state. In this mode, i_{LB}, i_{Lm}, and i_{Lr} keep increasing linearly with the same slope. In the meantime, C_{dc} and C_b continue to discharge and charge, respectively. At time t_2, S_w is turned OFF and the driver goes into the next mode.

Mode III [t_2–t_3, Fig. 4(c)]: The switches S_{o1}, S_{o2}, and S_{o3} are in ON-state, while the switch S_w is in OFF-state. At time t_2, i_{LB} begins to decrease linearly and C_{dc} begins to charge. However, i_{Lm} keeps increasing linearly with the same slope as L_m is still clamped by the voltage nV_{Cb} in this mode. Although i_{Lr} begins to decrease quickly, the value of i_{Lr} is still larger than i_{Lm}. Hence, C_b continues to charge, and C_{o1}, C_{o2}, and C_{o3} release energy to supply respective LED string. At time t_3, the values of i_{Lr} and i_{Lm} are equal and the driver goes into the next mode.

Mode IV [t_3–t_4, Fig. 4(d)]: The switches S_{o1}, S_{o2} are in ON-state, while the switch S_w and S_{o3} are in OFF-state. In this mode, i_{LB} continues to decrease linearly and C_{dc} continues to charge. Besides, i_{Lm} keeps increasing linearly with a smaller slope as L_m is clamped by the voltage $n(V_{Cb}-V_{o3})$. But i_{Lr} continues to decrease quickly, so that the value of i_{Lr} is smaller than i_{Lm}. Hence, C_b begins to discharge, and C_{o1} and C_{o2} release energy to supply respective LED string. At time t_4, i_{Lr} decreases to zero and D_r is turned OFF with zero current. At the same time, the driver goes into the next mode.

Mode V [t_4–t_5, Fig. 4(e)]: The switches S_{o1} and S_{o2} are in ON-state, while the switch S_w and S_{o3} are still in OFF-state. As described in mode IV, i_{LB} continues to decrease linearly, and i_{Lm} keeps increasing linearly with the same slope. Besides, C_b continues to discharge, and C_{o1} and C_{o2} release energy to supply respective LED string. At time t_5, S_{o2} is turned OFF and the driver goes into the next mode.

Mode VI [t_5–t_6, Fig. 4(f)]: The switch S_{o1} is in ON-state, while the switches S_w, S_{o2}, and S_{o3} are in OFF-state. As before, i_{LB} continues to decrease linearly with the same slope. But i_{Lm} begins to decrease linearly as L_m is clamped by the voltage

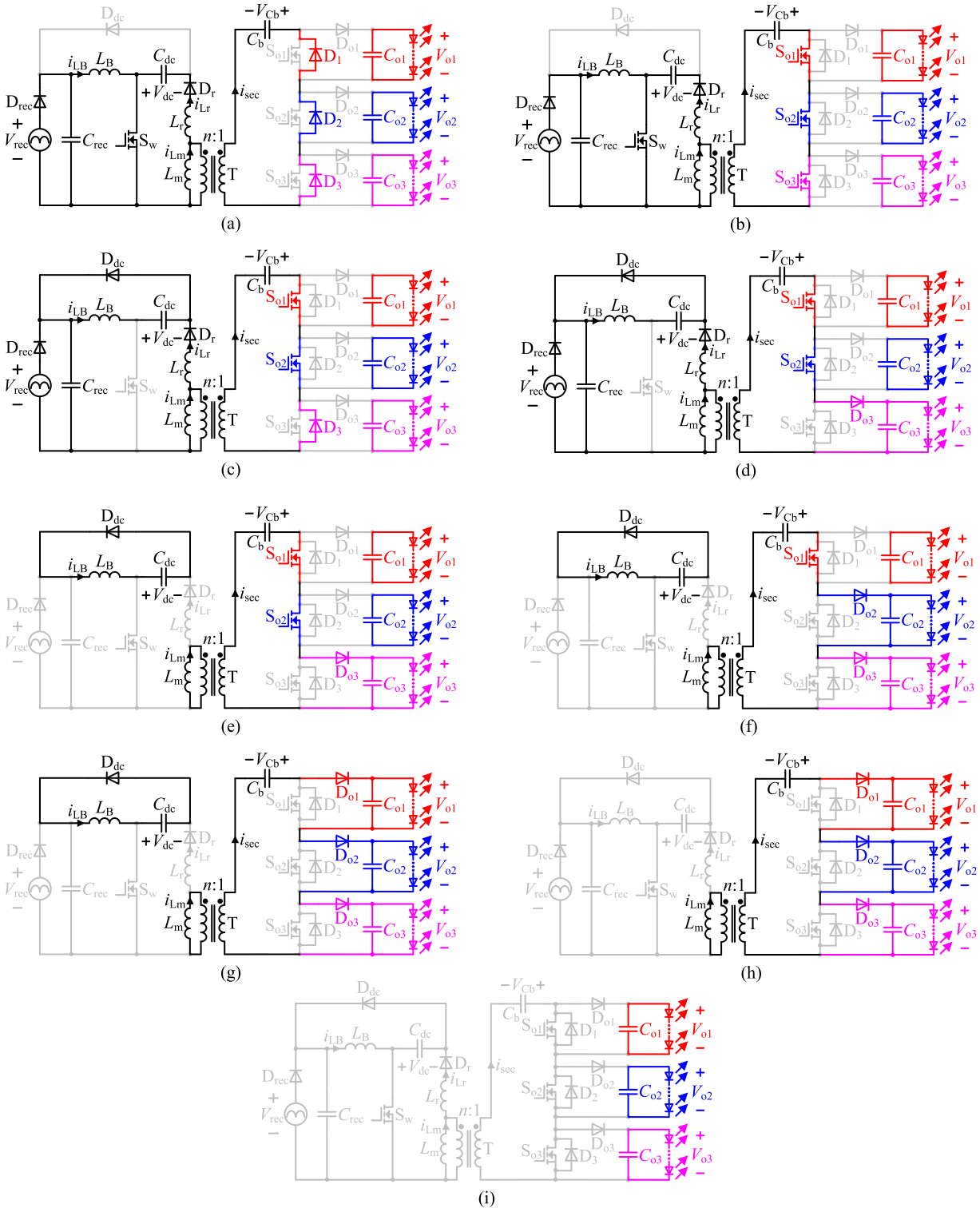

Fig. 4. Equivalent circuits for each operating mode. (a) Mode I. (b) Mode II. (c) Mode III. (d) Mode IV. (e) Mode V. (f) Mode VI. (g) Mode VII. (h) Mode VIII. (i) Mode IX.

$n(V_{\rm Cb}-V_{\rm o2}-V_{\rm o3})$ in this mode. Besides, $C_{\rm b}$ continues to discharge and $C_{\rm o1}$ releases energy to supply the first LED string. At time t_6, $S_{\rm o1}$ is turned OFF and the driver goes into the next mode.

Mode VII [t_6-t_7, Fig. 4(g)]: The switches $S_{\rm w}$, $S_{\rm o1}$, $S_{\rm o2}$, and $S_{\rm o3}$ are all in OFF-state. Likewise, $i_{\rm LB}$ continues to decrease linearly with the same slope. However, $i_{\rm Lm}$ keeps decreasing linearly with a larger slope as $L_{\rm m}$ is clamped by the voltage $n(V_{\rm Cb}-V_{\rm o1}-V_{\rm o2}-V_{\rm o3})$ in this mode, and $C_{\rm b}$ continues to discharge. At time t_7, $i_{\rm LB}$ decreases to zero and $D_{\rm dc}$ is turned OFF with zero current. At the same time, the driver goes into the next mode.

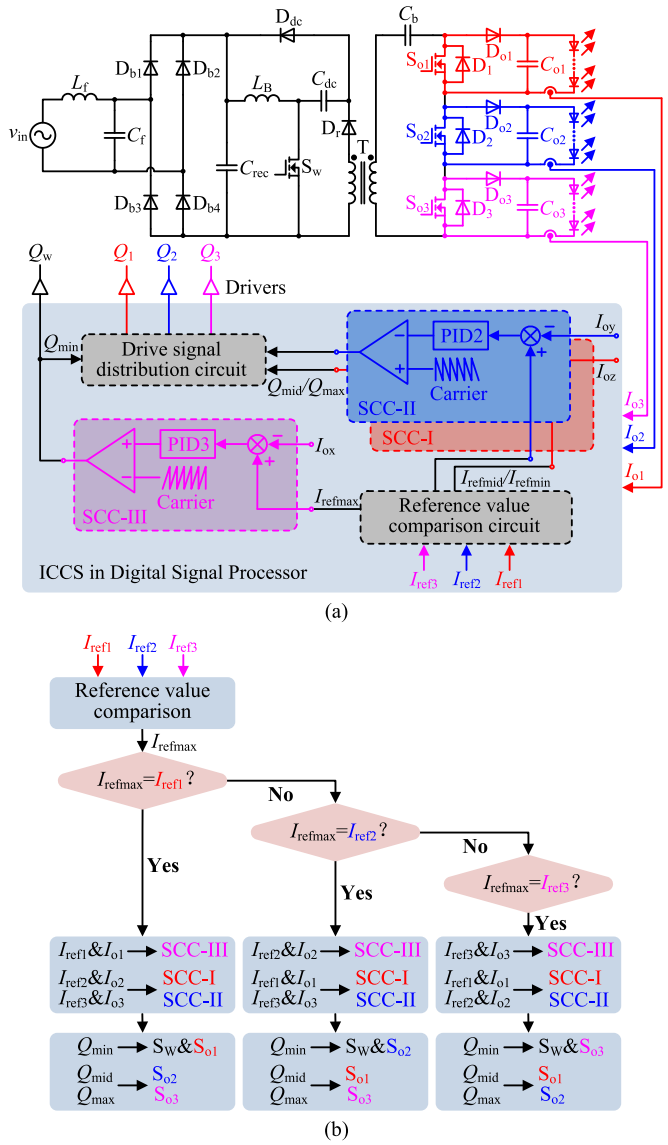

Fig. 5. Independent closed-loop control strategy (ICCS) of the proposed LED driver with $N = 3$. (a) Control schematic diagram. (b) Specific control flowchart.

Mode VIII [$t_7 - t_8$, Fig. 4(h)]: The switches S_w, S_{o1}, S_{o2}, and S_{o3} are all in OFF-state. In this mode, i_{LB} has decreased to zero and i_{Lm} keeps decreasing linearly with the same slope as the previous mode. At time t_8, i_{Lm} decreases to zero and D_{o1}, D_{o2}, and D_{o3} are all turned OFF with zero current. At the same time, the driver goes into the next mode.

Mode IX [$t_8 - t_9$, Fig. 4(i)]: The switches S_w, S_{o1}, S_{o2}, and S_{o3} are all in OFF-state. Both i_{LB} and i_{Lm} have decreased to zero in this mode, and C_{o1}, C_{o2}, and C_{o3} release energy to supply respective LED string again. At time t_9, S_w is turned ON with zero current again and the operation returns to Mode I of the next switching period.

III. Independent Closed-Loop Control Strategy

The ICCS of the proposed LED driver with $N = 3$ is illustrated in Fig. 5. Here, ICCS can be fully implemented in a DSP. Since AOU_1, AOU_2, and AOU_3 are series-connected, the input current of these three output units, that is the discharge current of the blocking capacitor C_b, is equal after the primary switch S_w is turned OFF. Intelligibly, the conduction time of D_{o1}, D_{o2}, and D_{o3} in a switching period can be changed by regulating the duty cycles of S_{o1}, S_{o2}, and S_{o3}, respectively. Therefore, the three output currents I_{o1}, I_{o2}, and I_{o3} can be controlled just by regulating the duty cycles of S_{o1}, S_{o2}, and S_{o3}. Thus, it is necessary to detect the three output currents to form independent close-loop control and regulate the duty cycles of S_{o1}, S_{o2}, and S_{o3} automatically. It is remarkable that current can flow through all output units at the same time, so the TDM control method is not necessary.

Clearly, as shown in Fig. 5(a), three independent single closed-loop control circuits (SCC) are always needed to produce the required drive signals of S_{o1}, S_{o2}, and S_{o3}, which are denoted as SCC-I, SCC-II, and SCC-III, respectively. Note that the structures of SCC-I and SCC-II are same, but different from the structure of SCC-III. In addition, the feedback current value I_{ox} in SCC-III denotes the current sampling value corresponding to the maximum reference value I_{refmax}, and then I_{oy}, I_{oz} denote the current sampling values corresponding to the other two reference values I_{refmid}/I_{refmin}. Hence, a reference value comparison circuit and a drive signal distribution circuit are also needed to obtain the maximum reference value I_{refmax} and further allocate the required drive signals to each power switch. For the conveniences of digital control, all of the above-mentioned functions can be fully programmed to implement in DSP.

The specific control flowchart of ICCS has been depicted in Fig. 5(b). For the sake of simplicity in the analysis, all the power switches S_w, S_{o1}, S_{o2}, and S_{o3} are considered to be turned ON synchronously. In ICCS, the three current reference values I_{ref1}, I_{ref2}, and I_{ref3} are compared to choose the maximum one I_{refmax} first. According to the comparative result, I_{refmax} and the corresponding output current sampling value will be sent into SCC-III to produce the minimum drive signal Q_{min}. Similarly, the other two current reference values I_{refmid}/I_{refmin} and corresponding output current sampling values will be sent into SCC-I/SCC-II to produce the drive signals Q_{mid} and Q_{max}. Finally, Q_{min}, Q_{mid}, and Q_{max} will be allocated to drive the power switches S_w, S_{o1}, S_{o2}, and S_{o3} automatically. For example, supposing that I_{ref3} is the maximum one and three reference values satisfy the following relationship: $I_{ref3} > I_{ref2} > I_{ref1}$. Therefore, $I_{ref3}/(I_{ox} = I_{o3})$ will be sent into SCC-III and $I_{ref2}/(I_{oy} = I_{o2})$, $I_{ref1}/(I_{oz} = I_{o1})$ will be sent into SCC-II, SCC-I, respectively. And then the three drive signals $Q_{min} = Q_{o3} = Q_w$, $Q_{mid} = Q_{o2}$, and $Q_{max} = Q_{o1}$ will be employed to drive S_w/S_{o3}, S_{o2}, S_{o1}, respectively. If the maximum current reference value is not I_{ref3}, the specific control process of ICCS is similar to the process above. Therefore, according to different values of I_{ref1}, I_{ref2}, and I_{ref3}, the duty cycles of three output-switches S_{o1}, S_{o2}, and S_{o3} can be adjusted automatically and always keep unequal. That is to say, the three output currents can be regulated independently.

IV. Parameter Design Method

The concretely quantitative design method of circuit parameters in the proposed LED driver with $N = 3$ are elaborated in

TABLE I
SPECIFICATION REQUIREMENTS OF THE PROPOSED LED DRIVER

Parameter	Value
Input voltage range $v_{\text{in(rms)}}$	198 V-242 V
Total output power P_{o}	120 W
1st output power P_{o1}	40 W
2nd output power P_{o2}	40 W
3rd output power P_{o3}	40 W
1st output current I_{o1} (Red)	500 mA
2nd output current I_{o2} (Green)	700 mA
3rd output current I_{o3} (Blue)	1000 mA
Switching frequency f_{s}	100 kHz

this section. For more effective research about parameter design process, some assumptions are made as below:

1) AC input voltage $v_{\text{in}}(t) = V_{\text{m}} \sin\omega t$ is an ideal sinusoidal voltage source, where V_{m} and ω are the amplitude and angular frequency, respectively.
2) All switches and diodes are regarded as ideal devices.
3) V_{dc}, V_{Cb}, V_{o1}, V_{o2}, and V_{o3} can remain unchanged since the values of C_{dc}, C_{b}, C_{o1}, C_{o2}, and C_{o3} are large enough.
4) The value of the magnetizing inductor L_{m} is much larger than the leakage inductor L_{r} in the equivalent model of the isolation transformer.
5) The switching frequency f_{s} is much higher than the line frequency f_{L}.

Here, taking $I_{\text{o1}} = 500$ mA, $I_{\text{o2}} = 700$ mA, and $I_{\text{o3}} = 1000$ mA as an example to discuss the parameter design method. Besides, the total output power is set at 120 W and the output power of each AOU is equal to 40 W. The specification requirements of the proposed LED driver with $N = 3$ are listed in Table I.

Note that $P_{\text{o1}} = P_{\text{o2}} = P_{\text{o3}} = 40$ W in Table I is just one of the output power distribution modes when the total output power is 120 W. For other cases, where the desired values of the three output currents or the output power distribution modes are different, the specific analysis processes are all same as above.

A. Design Considerations of L_{B}

According to [21], a unity power factor can be obtained if the Buck–Boost PFC unit operates in DCM and the duty ratio of S_{w} keeps constant during half line cycle. Thus, it is critical to choose a reasonable value of L_{B} to make sure that Buck–Boost PFC unit can be operated in DCM during the whole variation range of the input voltage. Further analysis indicates that Buck–Boost PFC unit always can be operated in DCM as long as it is operated in DCM when V_{rec} is equal to the peak value of the minimum input voltage. Hence, the maximum value of L_{B} should ensure that Buck–Boost PFC unit at least can operate in boundary conduction mode (BCM) at the peak point of the minimum input voltage. The quantitative relationship among L_{B}, V_{m}, P_{o1}, P_{o2}, and P_{o3} should be derived first, and then the maximum value of L_{B} in BCM can be obtained naturally.

The operating waveform of the inductor current i_{LB} at the minimum input voltage is depicted in Fig. 6. At the voltage peak point, it can be seen that the duty ratio d_1 should satisfy

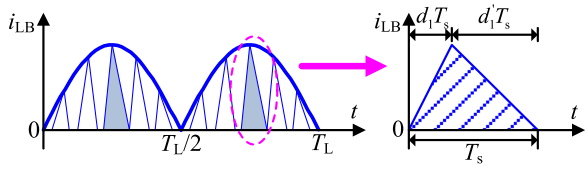

Fig. 6. Operating waveform of i_{LB} in BCM.

the following relationship since i_{LB} operates in BCM.

$$d_1 + d_1' = 1 \tag{1}$$

where d_1 is the duty ratio of the switch S_{w}.

Moreover, the inductor voltage should meet the volt-second balance principle in an entire switching period T_{s}, that is

$$V_{\text{m}} d_1 - V_{\text{dc}} d_1' = 0. \tag{2}$$

Based on (1) and (2), the duty ratio d_1 in BCM can be deduced as

$$d_1 = \frac{V_{\text{dc}}}{V_{\text{m}} + V_{\text{dc}}}. \tag{3}$$

Suppose that the efficiency of the proposed LED driver is 100%, namely, the input power is equal to the total output power, hence

$$P_{\text{o1}} + P_{\text{o2}} + P_{\text{o3}} = P_{\text{in}} = \frac{1}{2} V_{\boldsymbol{m}} I_{\text{inm}} \tag{4}$$

where I_{inm} is the amplitude of the input current i_{in}.

As derived in [21], I_{inm} can be expressed as

$$I_{\text{inm}} = \frac{V_{\text{m}} d_1^2 T_{\text{s}}}{2L_{\text{B}}}. \tag{5}$$

According to (4) and (5), the expression of L_{B} in BCM can be derived as

$$L_{\text{B}} = \frac{V_{\text{m}}^2 d_1^2 T_{\text{s}}}{4(P_{\text{o1}} + P_{\text{o2}} + P_{\text{o3}})}. \tag{6}$$

Since d_1 is the duty ratio of S_{w} in BCM, the obtained value of L_{B} according to (6) is the critical value $L_{\text{B(BCM)}}$, which is also the maximum value of L_{B}. It can be inferred that d_1 will decrease along with the increasing of the input voltage amplitude V_{m} once the value of L_{B} has been determined. The duty ratio d_1 reaches its maximum value $d_{1\max}$ when the input voltage is equal to its minimum value. Therefore, to calculate the critical inductance $L_{\text{B(BCM)}}$, it is necessary to determine the maximum duty ratio $d_{1\max}$ in advance.

According to (6), it is believed that the duty ratio d_1 will decrease along with the decreasing of the total output power during the dimming process. Here, the dimming process is referred to the average value of each output current can be regulated below the corresponding maximum value. In other words, the inductor L_{B} should always operate in DCM during the dimming process. Hence, the value of L_{B} is designed in the condition of the total output power is maximum, which can ensure the designed value of L_{B} still be valid and effective within the dimming process.

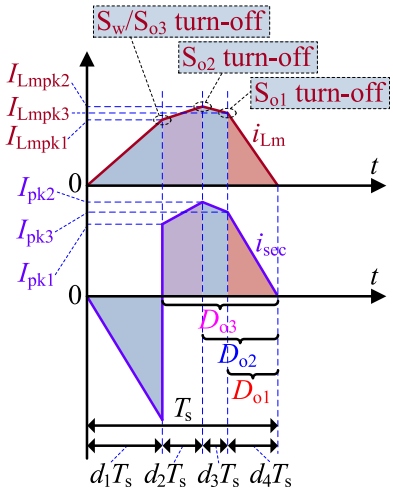

Fig. 7. Operating waveforms of i_{Lm} and i_{sec} in BCM.

B. Design Considerations of L_{m} and n

As described in Part II, the three diodes D_{o1}, D_{o2}, and D_{o3} all can be turned OFF with zero current when the magnetizing inductor current i_{Lm} is also designed to operate in DCM, so that it can reduce reverse recovery losses and improve conversion efficiency. Similar to the design considerations of L_{B}, if the magnetizing inductor L_{m} can operate in BCM when the duty ratio d_1 is equal to its maximum value $d_{1\max}$, L_{m} will always operate in DCM along with the increasing of the input voltage. Similarly, note that the magnetizing inductor L_{m} will also always operate in DCM during the dimming process as long as L_{m} can operate in DCM when $P_{\mathrm{o1}} = P_{\mathrm{o2}} = P_{\mathrm{o3}} = 40$ W. Therefore, the value of L_{m} is also designed in the condition of the three output powers P_{o1}, P_{o2}, and P_{o3} are maximum, respectively.

Similarly, the quantitative relationship among L_{B}, V_{m}, P_{o1}, P_{o2}, and P_{o3} in BCM should be derived primarily. Then, it can further calculate the main parameters (that is, L_{m} and n) of the isolation transformer in BCM. The operating waveforms of i_{Lm} and i_{sec} in an entire switching period T_{s} are sketched in Fig. 7 for the BCM, where i_{sec} is the secondary side current of the transformer. Obviously, there are two current ramp-up subintervals and two current ramp-down subintervals in a switching period T_{s} about the waveform of i_{Lm}. The turn-OFF moments of $S_{\mathrm{w}}/S_{\mathrm{o3}}$ correspond to the first slope turning point in the waveform of i_{Lm}. Additionally, the turn-OFF moments of S_{o2} and S_{o1} correspond to the other two slope turning points. Hence, an entire switching period T_{s} can be divided into four subintervals that are d_1T_{s}, d_2T_{s}, d_3T_{s}, and d_4T_{s}.

As shown in Fig. 7, the conduction time of the diode D_{o3} in AOU_3 is $(d_2 + d_3 + d_4)T_{\mathrm{s}}$, and the average current flows through D_{o3} is equal to the average output current I_{o3} since the average current of C_{o3} is equal to zero. In addition, the conduction time of the diodes D_{o2}, D_{o1} are $(d_3 + d_4)T_{\mathrm{s}}$, d_4T_{s}, respectively. The average currents of D_{o2} and D_{o1} are equal to the average output currents I_{o2} and I_{o1}. Hence, the following three equations can be established.

$$\frac{1}{2}I_{\mathrm{pk3}} \cdot d_4 = I_{\mathrm{o1}} \tag{7}$$

$$\frac{1}{2}(I_{\mathrm{pk2}} + I_{\mathrm{pk3}}) \cdot d_3 = I_{\mathrm{o2}} - I_{\mathrm{o1}} \tag{8}$$

$$\frac{1}{2}(I_{\mathrm{pk1}} + I_{\mathrm{pk2}}) \cdot d_2 = I_{\mathrm{o3}} - I_{\mathrm{o2}} \tag{9}$$

where I_{pk1}, I_{pk2}, and I_{pk3} are the inflectional values of the secondary side current i_{sec} at the turn-OFF moments of $S_{\mathrm{w}}/S_{\mathrm{o3}}$, S_{o2}, and S_{o1}, respectively.

Since the value of inductance L_{r} is much smaller than L_{m}, the decreasing time of the leakage inductor current i_{Lr} can be neglected. It can be believed that i_{Lr} decreases to zero immediately after S_{w} is turned OFF. Therefore, I_{pk1}, I_{pk2}, and I_{pk3} can be expressed as

$$I_{\mathrm{pk1}} = nI_{\mathrm{Lmpk1}} = n\frac{V_{\mathrm{dc}}}{L_{\mathrm{m}}}d_1T_{\mathrm{s}} \tag{10}$$

$$I_{\mathrm{pk2}} = nI_{\mathrm{Lmpk2}} = n\left[\frac{n(V_{\mathrm{Cb}} - V_{\mathrm{o3}})}{L_{\mathrm{m}}}d_2T_{\mathrm{s}} + I_{\mathrm{Lmpk1}}\right] \tag{11}$$

or

$$I_{\mathrm{pk2}} = nI_{\mathrm{Lmpk2}} = n\left[\frac{n(V_{\mathrm{o2}} + V_{\mathrm{o3}} - V_{\mathrm{Cb}})}{L_{\mathrm{m}}}d_3T_{\mathrm{s}} + I_{\mathrm{Lmpk3}}\right] \tag{12}$$

$$I_{\mathrm{pk3}} = nI_{\mathrm{Lmpk3}} = \frac{n^2(V_{\mathrm{o1}} + V_{\mathrm{o2}} + V_{\mathrm{o3}} - V_{\mathrm{Cb}})}{L_{\mathrm{m}}}d_4T_{\mathrm{s}} \tag{13}$$

where I_{Lmpk1}, I_{Lmpk2}, and I_{Lmpk3} are the inflectional values of the magnetizing inductor current i_{Lm} at the turn-OFF moments of $S_{\mathrm{w}}/S_{\mathrm{o3}}$, S_{o2}, and S_{o1}, respectively.

The primary side voltage and the secondary side voltage of the transformer are equal to the voltages across C_{dc} and C_{b} when S_{w} is turned ON, respectively. Hence, V_{dc} and V_{Cb} should meet the following relationship in this interval.

$$V_{\mathrm{dc}} = nV_{\mathrm{Cb}}. \tag{14}$$

Solving (7), (13), and (14) yields

$$d_4 = \sqrt{\frac{2L_{\mathrm{m}}I_{\mathrm{o1}}}{[n^2(V_{\mathrm{o1}} + V_{\mathrm{o2}} + V_{\mathrm{o3}}) - nV_{dc}]\,T_{\mathrm{s}}}} \tag{15}$$

$$I_{\mathrm{pk3}} = \sqrt{\frac{2I_{\mathrm{o1}}T_{\mathrm{s}}\,[n^2(V_{\mathrm{o1}} + V_{\mathrm{o2}} + V_{\mathrm{o3}}) - nV_{dc}]}{L_{\mathrm{m}}}}. \tag{16}$$

Solving (8), (12), and (14) yields

$$d_3 = \frac{\sqrt{{I_{\mathrm{pk3}}}^2 + 2A(I_{o2} - I_{o1})} - I_{\mathrm{pk3}}}{A} \tag{17}$$

$$I_{\mathrm{pk2}} = \frac{2A(I_{o2} - I_{o1})}{\sqrt{{I_{\mathrm{pk3}}}^2 + 2A(I_{o2} - I_{o1})} - I_{\mathrm{pk3}}} - I_{\mathrm{pk3}} \tag{18}$$

where $A = \frac{[n^2(V_{\mathrm{o2}} + V_{\mathrm{o3}}) - nV_{\mathrm{dc}}]T_{\mathrm{s}}}{L_{\mathrm{m}}}$.

According to (9) and (10), the duty ratio d_2 can be expressed as

$$d_2 = \frac{2(I_{o3} - I_{o2})}{n\frac{V_{\mathrm{dc}}}{L_{\mathrm{m}}}d_1T_{\mathrm{s}} + I_{\mathrm{pk2}}}. \tag{19}$$

TABLE II
VOLTAGE STRESSES OF MAIN SWITCHING DEVICES

Switching device	Voltage stress
S_w/D_{dc}	$V_{m(max)}+V_{dc}$
D_r	$V_{m(max)}+n(V_{Cb}-V_{o3})$
S_{o1}/D_{o1}	V_{o1}
S_{o2}/D_{o2}	V_{o2}
S_{o3}/D_{o3}	V_{o3}

Similarly, the magnetizing inductor voltage should also meet the volt-second balance principle in an entire switching period T_s, that is

$$V_{dc}d_1 + n\,(V_{Cb} - V_{o3})\,d_2 = n(V_{o2} + V_{o3} - V_{Cb})d_3 + n(V_{o1} + V_{o2} + V_{o3} - V_{Cb})d_4. \quad (20)$$

Besides, the duty ratios d_1, d_2, d_3, and d_4 in BCM should satisfy the following equation.

$$d_1 + d_2 + d_3 + d_4 = 1. \quad (21)$$

Substituting (14)–(19) into (20) yields

$$f_1(L_m, n) = 0. \quad (22)$$

Substituting (14)–(19) into (21) yields

$$f_2(L_m, n) = 0. \quad (23)$$

Obviously, (22) and (23) are both binary non-linear equations related to L_m and n, where d_1 is equal to its maximum value d_{1max}. Therefore, the critical magnetizing inductance $L_{m(BCM)}$ and turns ratio $n_{(BCM)}$ in BCM can also be obtained finally by solving (22) and (23) simultaneously. Certainly, d_{1max} also need to be determined beforehand.

C. Quantitative Determination of d_{1max}

According to the operating mode analysis above, the voltage stresses of main switching devices can be listed in Table II, where V_{o1}, V_{o2}, and V_{o3} are the average values of three-channel output voltages, respectively. It can be observed that the maximum voltage stress on S_w is equal to $V_{m(max)}+V_{dc}$, which is the maximum one compared with the voltage stresses on the other switching devices. Here, $V_{m(max)}$ is the amplitude of the maximum input voltage.

Taking the withstand voltage of silicon MOSFET into consideration, the maximum voltage stress on S_w is expected to be less than 500 V within the whole variation ranges of the input voltage. That is, the average energy-stored capacitor voltage V_{dc} should be limited to less than 158 V. The duty ratio of S_w that satisfies this limited condition is the reasonable maximum duty ratio d_{1max}.

The flowchart for determining the maximum duty ratio d_{1max} is illustrated in Fig. 8. According to the preset parameters as listed in Table I, the concrete quantitative determination process of d_{1max} is presented in detail as follows.

First, the variation range of d_1 is preset to 0.3–0.4 with taking 0.01 as the step-length in this range. According to (6), 11 critical values of inductance L_B, that is $L_{B(BCM)}$, can be calculated out

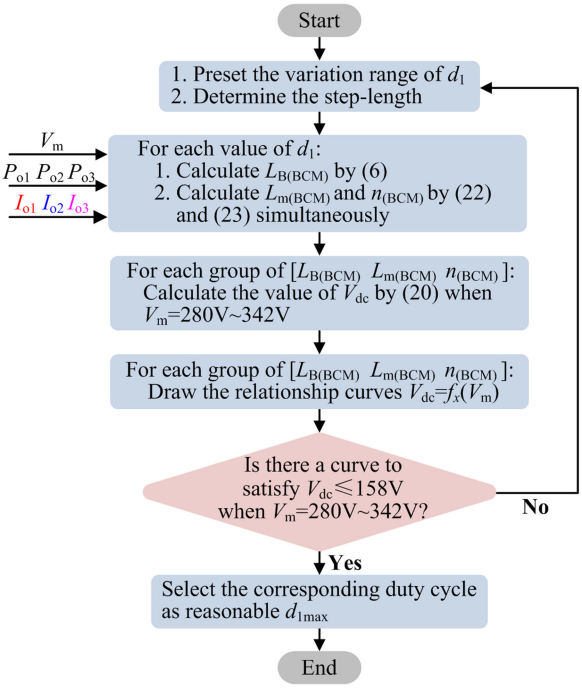

Fig. 8. Flowchart for determining d_{1max}.

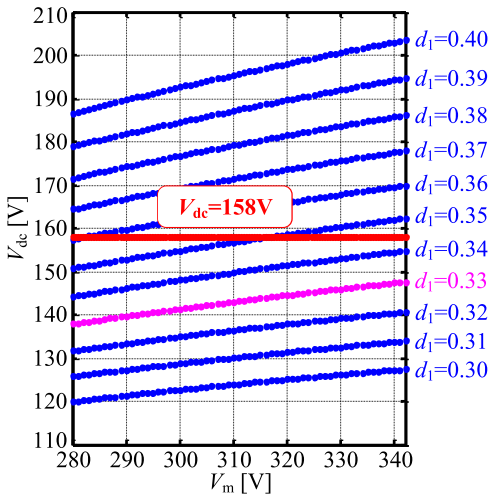

Fig. 9. Eleven relation curves among V_{dc} and V_m with V_m = 280–342 V.

with V_m = 280 V and P_{o1} = P_{o2} = P_{o3} = 40 W. Besides, 11 groups of $L_{m(BCM)}$ and $n_{(BCM)}$ can be calculated out with the same conditions by (22) and (23). And then the 11 groups of $L_{B(BCM)}$, $L_{m(BCM)}$, and $n_{(BCM)}$ above can be, respectively, taken into (20) to calculate out the corresponding values of V_{dc} when V_m varies from 280 to 342 V. Finally, 11 relation curves among V_{dc} and V_m, that is, V_{dc} = $f_x(V_m)$, where x = 1, 2, . . . , 11, can be drawn in Fig. 9 simultaneously.

As shown in Fig. 9, the energy-stored capacitor voltage V_{dc} will be less than 158 V when V_m varies from 280 to 342 V as long as the duty ratio $d_1 \leq 0.34$. To avoid the problem that the smaller duty ratio will cause excessive current stresses of the switching devices, d_{1max} = 0.33 is a proper choice for the maximum duty ratio.

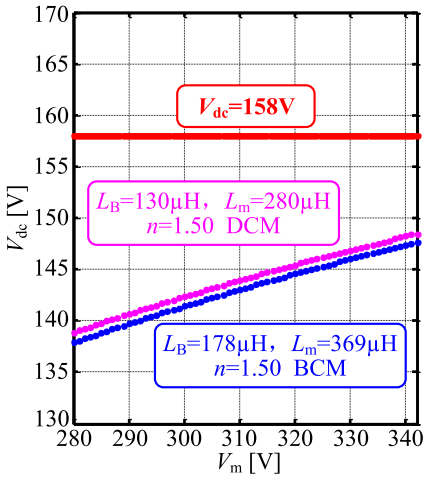

Fig. 10. Two relation curves among $V_{\rm dc}$ and $V_{\rm m}$ in BCM and DCM.

D. Quantitative Calculation of $L_{\rm B}$, $L_{\rm m}$, n, and Verification

As previously mentioned, the values of $L_{\rm B}$, $L_{\rm m}$, and n in BCM can be quantitatively calculated out as long as the maximum duty ratio $d_{1\max}$ has been determined at first.

Substituting $d_{1\max} = 0.33$ and $V_{\rm m} = 280$ V into (6), (22), and (23), the critical values of $L_{\rm B}$, $L_{\rm m}$, and n can be calculated out, that is, $L_{\rm B(BCM)} = 178\ \mu$H, $L_{\rm m(BCM)} = 369\ \mu$H, and $n_{\rm (BCM)} = 1.50$. To ensure the inductor $L_{\rm B}$ and the magnetizing inductor $L_{\rm m}$ both operate in DCM with enough allowance, $L_{\rm B} = 130\ \mu$H, $L_{\rm m} = 280\ \mu$H, and $n = 1.50$ are eventually chosen.

The following is to verify whether or not $V_{\rm dc}$ will be less than 158 V within the whole variation ranges of the input voltage after determining the values of $L_{\rm B}$, $L_{\rm m}$, and n. The two relation curves among $V_{\rm dc}$ and $V_{\rm m}$ in BCM and DCM are both drawn in Fig. 10, where $V_{\rm m}$ varies from 280 to 342 V. Obviously, the value of $V_{\rm dc}$ in DCM has increased compared with the value in BCM. However, the increase amount is relatively slight that still can ensure $V_{\rm dc} \le 158$ V when $V_{\rm m}$ varies from 280 to 342 V. Hence, the parameters $L_{\rm B} = 130\ \mu$H, $L_{\rm m} = 280\ \mu$H, and $n = 1.50$ are reasonable for the proposed LED driver with $N = 3$.

E. Design Considerations of $C_{\rm dc}$

The twice line frequency ripple voltage $\Delta v_{\rm dc}(t)$ on the energy-stored capacitor $C_{\rm dc}$ is needed to be derived out according to the current flows through $C_{\rm dc}$ at first. Then, the ripple voltage peak-to-peak value $\Delta V_{\rm dc}$ can be obtained naturally. According to the design objective of $\Delta V_{\rm dc}$, the quantitative value of $C_{\rm dc}$ can be calculated out finally.

As illustrated in Fig. 2, the average value of $i_{\rm Cdc}$ is equal to the difference between the average values of $i_{\rm LB}$ and $i_{\rm Sw}$ in a switching period, that is

$$\bar{i}_{C_{\rm dc}}(t) = \bar{i}_{\rm LB}(t) - \bar{i}_{\rm S_w}(t). \tag{24}$$

In (24), the average current $\bar{i}_{\rm LB}(t)$ in a switching period can be expressed as

$$\bar{i}_{\rm LB}(t) = \frac{V_{\rm m} d_1^2 T_{\rm s}}{2L_{\rm B}} |\sin \omega t| \left(1 + \frac{V_{\rm m}}{V_{\rm dc}} |\sin \omega t|\right). \tag{25}$$

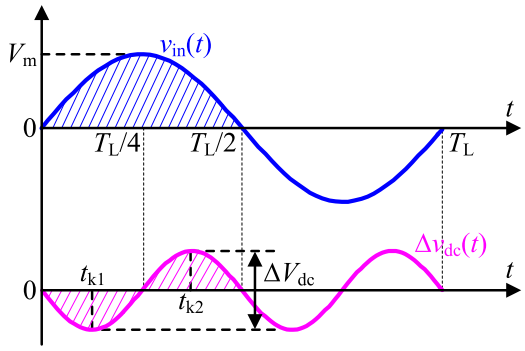

Fig. 11. Waveforms of the input voltage $v_{\rm in}(t)$ and ripple voltage $\Delta v_{\rm dc}(t)$.

Based on the ampere-second balance principle, the average current through the output-switch $S_{\rm o3}$ in $\rm AOU_3$ is equal to the average output current $I_{\rm o3}$. Consequently, the peak value of the switch current $i_{\rm So3}$ at the turn-OFF moment of $S_{\rm w}$ can be expressed as

$$I_{\rm So3pk} = \frac{2I_{\rm o3}}{d_1}. \tag{26}$$

Furthermore, the peak value of $i_{\rm Sw}$ at the turn-OFF moment of $S_{\rm w}$ can be derived as

$$i_{\rm Swpk}(t) = \frac{V_{\rm m} d_1 T_{\rm s}}{L_{\rm B}} |\sin \omega t| + \frac{V_{\rm dc} d_1 T_{\rm s}}{L_{\rm m}} + \frac{2I_{\rm o3}}{n d_1}. \tag{27}$$

Accordingly, the average value of $i_{\rm Sw}$ in a switching period can be deduced, that is

$$\bar{i}_{S_{\rm w}}(t) = \frac{V_{\rm m} d_1^2 T_{\rm s}}{2L_{\rm B}} |\sin \omega t| + \frac{V_{\rm dc} d_1^2 T_{\rm s}}{2L_{\rm m}} + \frac{I_{\rm o3}}{n}. \tag{28}$$

Substituting (25) and (28) into (24) can obtain the expression of $\bar{i}_{C_{\rm dc}}(t)$ in a switching period, that is

$$\bar{i}_{C_{\rm dc}}(t) = \frac{V_{\rm m}^2 d_1^2 T_{\rm s}}{2L_{\rm B} V_{\rm dc}} \sin^2 \omega t - \left(\frac{V_{\rm dc} d_1^2 T_{\rm s}}{2L_{\rm m}} + \frac{I_{\rm o3}}{n}\right). \tag{29}$$

According to (29), the twice line frequency ripple voltage on $V_{\rm dc}$ in half line cycle can be calculated as

$$\Delta v_{\rm dc}(t) = \frac{1}{C_{\rm dc}} \int_0^t [\bar{i}_{\rm Cdc}(t)] {\rm d}t \tag{30}$$

where $0 \le t \le T_{\rm L}/2$ and $T_{\rm L}$ is the line cycle, that is $T_{\rm L} = 1/f_{\rm L}$.

The waveforms of the input voltage $v_{\rm in}(t)$ and ripple voltage $\Delta v_{\rm dc}(t)$ in a line cycle are depicted in Fig. 11. It can be seen that the ripple voltage peak-to-peak value $\Delta V_{\rm dc}$ is equal to the difference between the maximum value and minimum value of $\Delta v_{\rm dc}(t)$.

As shown in Fig. 11, the differential of $\Delta v_{\rm dc}(t)$ should be equal to zero at the moment $t_{\rm k2}$ when $\Delta v_{\rm dc}(t)$ reaches its maximum value. Hence, the value of $t_{\rm k2}$ can be derived as

$$t_{\rm k2} = \frac{\pi}{\omega} - \frac{1}{\omega} \arcsin \sqrt{\frac{V_{\rm dc}^2 L_{\rm B}}{V_{\rm m}^2 L_{\rm m}} + \frac{2I_{\rm o3} V_{\rm dc} L_{\rm B}}{n V_{\rm m}^2 d_1^2 T_{\rm s}}}. \tag{31}$$

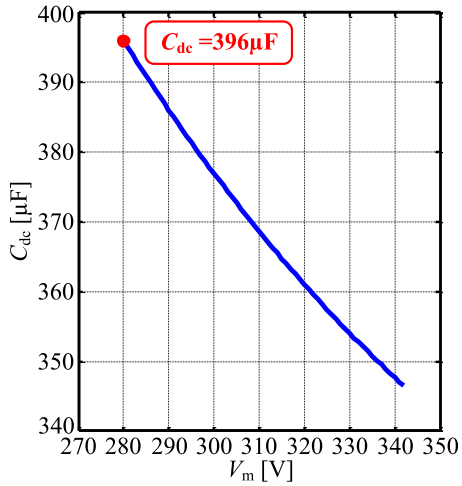

Fig. 12. Relation curve among C_{dc} and V_m with $V_m = 280$–342 V.

According to (29), (30), and (31), the ripple voltage peak-to-peak value ΔV_{dc} can be calculated as follows:

$$\begin{aligned}\Delta V_{dc} &= 2\Delta v_{dc}(t_{k2}) = \frac{2}{C_{dc}}\int_0^{t_{k2}} [\bar{i}_{Cdc}(t)]\,dt \\ &= \left(\frac{V_m^2 d_1^2 T_s}{2L_B C_{dc} V_{dc}} - \frac{V_{dc} d_1^2 T_s}{L_m C_{dc}} - \frac{2I_{o3}}{nC_{dc}}\right) t_{k2} \\ &\quad - \frac{V_m^2 d_1^2 T_s}{4\omega L_B C_{dc} V_{dc}} \sin(2\omega t_{k2}). \end{aligned} \tag{32}$$

Here, the value of C_{dc} should ensure that the ratio between ΔV_{dc} and the average energy-stored capacitor voltage V_{dc} will be less than 5% when V_m varies from 280 to 342 V. According to (32), taking $\Delta V_{dc}/V_{dc} = 5\%$, the relation curve among C_{dc} and V_m can be drawn in Fig. 12 after the values of L_B, L_m, and n all have been determined. Apparently, the value of C_{dc} will decrease gradually along with the increasing of V_m. To ensure the ratio $\Delta V_{dc}/V_{dc}$ can always be less than 5% within the whole variation ranges of V_m, the value of C_{dc} should equal to its maximum value. As shown in Fig. 12, the maximum value of C_{dc} is 396 μF when $V_m = 280$ V. Taking the nominal value of electrolytic capacitor into consideration, $C_{dc} = 470$ μF is eventually chosen.

V. Experimental Results

A 120 W digital-controlled experimental prototype with three-channel outputs has been built and tested to verify the effectiveness of the proposed LED driver with ICCS control method, as well as the correctness of parameter design method. The final designed parameters and selected components of the implemented prototype are summarized in Table III. Besides, the photograph of the experimental prototype is shown in Fig. 13, where the LEDs with R, G, and B color are used for three LED channels in the experimental prototype, respectively.

The steady-state experimental waveforms when $v_{in(rms)} = 220$ V are illustrated in Fig. 14. Here, three current reference values are set as follows: $I_{ref1} = 500$ mA, $I_{ref2} = 700$ mA, and $I_{ref3} = 1000$ mA. The experimental waveforms of v_{in}, i_{in},

TABLE III
Designed Parameters and Selected Components of the Prototype

Symbol	Definition	Value or Description
L_f	Input filter inductor	600 μH
C_f	Input filter capacitor	0.1 μF/630 V
C_{rec}	Snubber capacitor	22 nF/400 V
L_B	Inductor	130 μH
C_{dc}	Energy-stored capacitor	470 μF/250 V
L_m	Magnetizing inductor	280 μH
L_r	Leakage inductor	5 μH
n	Turns ratio	1.5 (15:10)
C_b	Blocking capacitor	10 μF/250 V
C_{o1}-C_{o3}	Output filter capacitors	(10 μF*2=20 μF)/100 V
S_w	Primary switch	IPP80R280P7 800 V/17 A
S_{o1}-S_{o3}	Output-switches	IPP530N15N3G 150 V/21 A
D_{b1}-D_{b4}	Rectifier diodes	STTH5R06 600 V/5 A
D_{dc}	Free-wheeling diode	STTH15L06 600 V/15 A
D_r	Blocking diode	STTH15L06 600 V/15 A
D_{o1}-D_{o3}	Output-diodes	SS515 150 V/5 A
LED	Output Loads	Cree® XLamp® XP-E LEDs Red: 500 mA/2.10 V 1.05 W Green: 700 mA/3.34 V 2.34 W Blue: 1000 mA/3.10 V 3.10 W

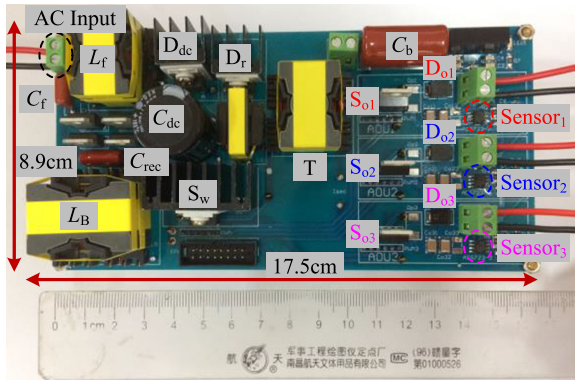

Fig. 13. Photograph of the experimental prototype.

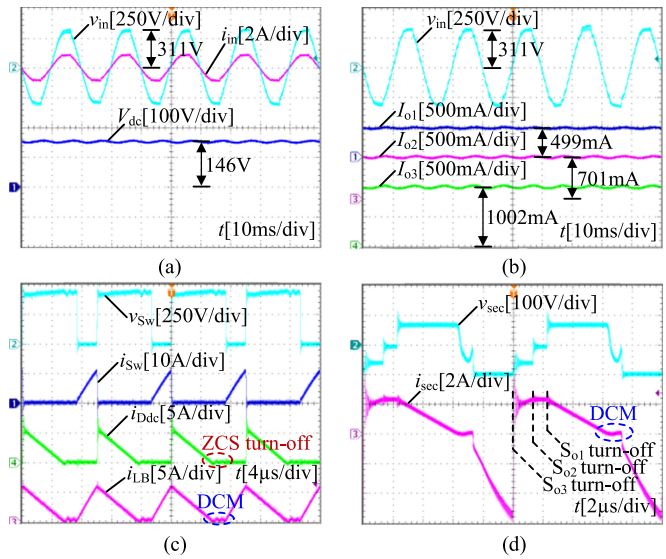

Fig. 14. Steady-state experimental waveforms when $v_{in(rms)} = 220$ V. (a) v_{in}, i_{in}, and V_{dc}. (b) v_{in}, I_{o1}, I_{o2}, and I_{o3}. (c) v_{Sw}, i_{Sw}, i_{Ddc}, and i_{LB}. (d) v_{sec}, i_{sec}.

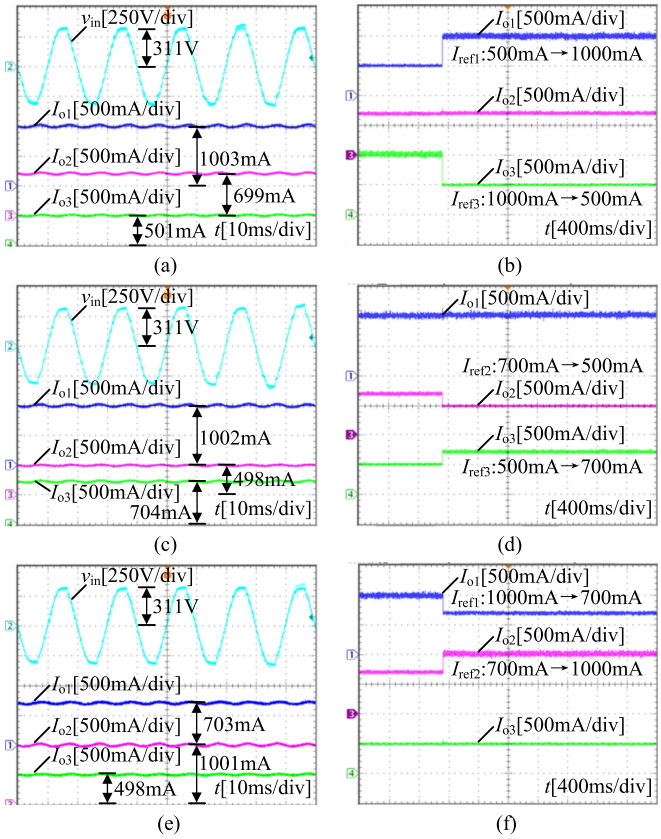

Fig. 15. Steady-state and dynamic experimental waveforms of I_{o1}, I_{o2}, and I_{o3} with different current reference values. (a) $I_{ref1} = 1000$ mA, $I_{ref2} = 700$ mA, $I_{ref3} = 500$ mA. (b) I_{ref1}: 500 mA→1000 mA, $I_{ref2} = 700$ mA, I_{ref3}: 1000 mA→500 mA. (c) $I_{ref1} = 1000$ mA, $I_{ref2} = 500$ mA, $I_{ref3} = 700$ mA. (d) $I_{ref1} = 1000$ mA, I_{ref2}: 700 mA→ 500 mA, I_{ref3}: 500 mA→700 mA. (e) $I_{ref1} = 700$ mA, $I_{ref2} = 1000$ mA, $I_{ref3} = 500$ mA. (f) I_{ref1}: 1000 mA→700 mA, I_{ref2}: 700 mA→1000 mA, I_{ref3}: 500 mA.

and V_{dc} are all shown in Fig. 14(a). It indicates that v_{in} and i_{in} are almost in phase to obtain high power factor, and measured power factor is equal to 0.998 in this case. Meanwhile, the average value of V_{dc} is equal to 146 V which is not more than 158 V. Fig. 14(b) shows the experimental waveforms of v_{in}, I_{o1}, I_{o2}, and I_{o3}, where the average values of three output currents are equal to 499, 701, 1002 mA, respectively. That is to say, I_{o1}, I_{o2}, and I_{o3} can keep constant and unequal as I_{ref1}, I_{ref2}, and I_{ref3} are different from each other. Fig. 14(c) shows the experimental waveforms of v_{Sw}, i_{Sw}, i_{Ddc}, and i_{LB}, where v_{Sw} is the voltage across the switch S_w, and i_{Sw}, i_{Ddc} are the currents flow through S_w and D_{dc}, respectively. It can be seen that the maximum voltage stress of S_w is not larger than 500 V as expected. Besides, the inductor current i_{LB} operates in DCM and the diode D_{dc} is turned OFF with zero current. Fig. 14(d) shows the experimental waveforms of v_{sec} and i_{sec}, where the secondary side current i_{sec} operates in DCM as expected. During the subinterval when S_w is turned OFF, the three inflection points correspond to the turn-OFF moments of S_{o3}, S_{o2}, and S_{o1} respectively, which is consistent with the theoretical analysis processes.

The steady-state and corresponding dynamic experimental waveforms of I_{o1}, I_{o2}, and I_{o3} with different current reference values are tested and presented in Fig. 15. According to

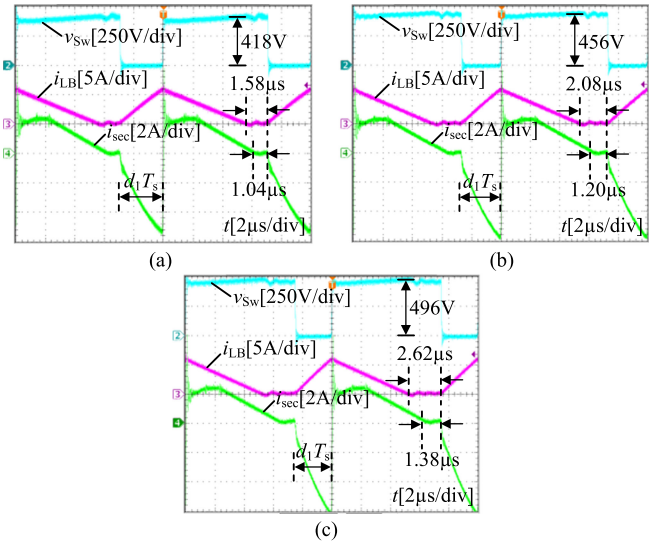

Fig. 16. Experimental waveforms of v_{Sw}, i_{LB}, and i_{sec} with different $v_{in(rms)}$. (a) $v_{in(rms)} = 198$ V. (b) $v_{in(rms)} = 220$ V. (c) $v_{in(rms)} = 242$ V.

Fig. 15(a), (c), and (e), it is observed that each output current can be automatically regulated to follow the corresponding current reference value after I_{ref1}, I_{ref2}, and I_{ref3} changed. That is, fully independent control of I_{o1}, I_{o2}, and I_{o3} can be achieved according to different current reference values, which are in agreement with the analysis. In addition, the dynamic experimental waveforms of I_{o1}, I_{o2}, and I_{o3} in Fig. 15(b), (d), and (f) shows that the average value of the remaining output current will not change after the step exchange of other two output currents. Therefore, zero cross-regulation can be achieved in the proposed series-type LED driver, and the independent closed-loop control system can remain stable.

The experimental waveforms of v_{Sw}, i_{LB}, and i_{sec} when $v_{in(rms)} = 198$, 220, and 242 V are illustrated in Fig. 16(a)–(c), respectively. It can be seen that the voltage stress of S_w changes from 418 to 496 V when $v_{in(rms)}$ varies from 198 to 242 V, which is always not more than 500 V. Another point worth noting is that i_{LB} and i_{sec} (that is, i_{Lm}) both operate in DCM during the whole variation ranges of $v_{in(rms)}$ as expected. The length of the intervals when i_{LB} and i_{sec} are equal to zero will increase along with the increasing of $v_{in(rms)}$, while the length of the interval d_1T_s will decrease as described in theory. Due to the increase amount of the input voltage amplitude V_m is more dramatically than the average value of V_{dc}, the length of the zero-value interval in i_{LB} waveform increases from 1.58 to 2.62 μs, while the length of this interval in i_{sec} waveform increases from 1.04 to 1.38 μs. All of these can verify the correctness of the theoretical analysis and the reasonability of parameter design results about L_B, L_m, and n.

The experimental waveforms of v_{in} and V_{dc} when $v_{in(rms)} = 198$, 220, and 242 V are illustrated in Fig. 17(a)–(c), respectively. Obviously, the average value of V_{dc} is always not more than 158 V that can satisfy the limitation above. Meanwhile, the ratio between the ripple voltage peak-to-peak value ΔV_{dc} and the average value of V_{dc} (that is, $\Delta V_{dc}/V_{dc}$) decreases from 4.71% to 3.57% when $v_{in(rms)}$ varies from 198 to 242 V, which

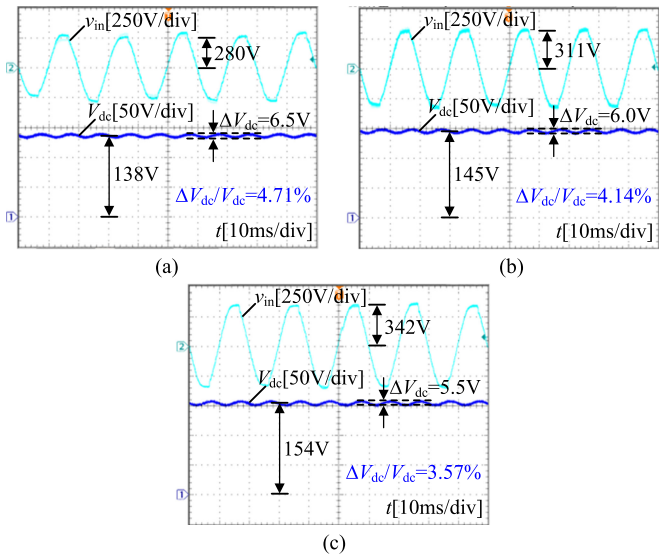

Fig. 17. Experimental waveforms of $v_{\rm in}$ and $V_{\rm dc}$ with different $v_{\rm in(rms)}$. (a) $v_{\rm in(rms)} = 198$ V. (b) $v_{\rm in(rms)} = 220$ V. (c) $v_{\rm in(rms)} = 242$ V.

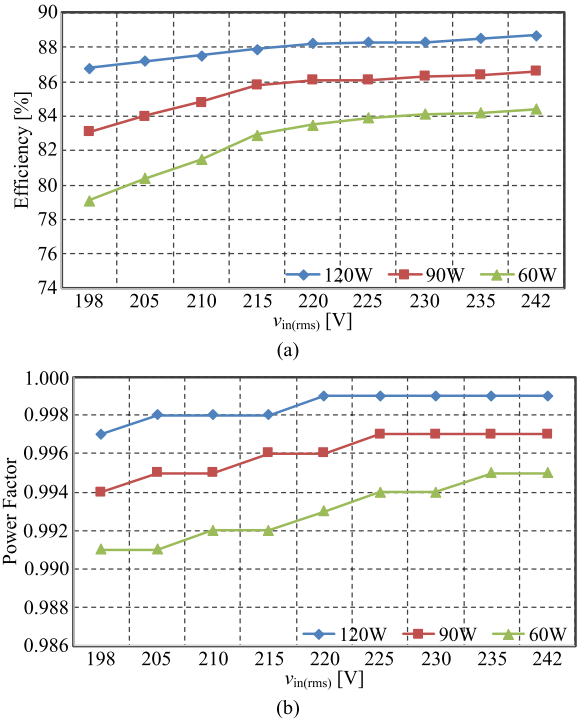

Fig. 18. Measured efficiency curves and PF curves with $v_{\rm in(rms)} = 198$–242 V. (a) Efficiency curves at $P_{\rm o} = 120$, 90, and 60 W. (b) PF curves at $P_{\rm o} = 120$, 90, and 60 W.

is always less than 5%. Hence, the design value of the energy-stored capacitor $C_{\rm dc}$ is also reasonable and effective.

The measured efficiency curves and PF curves at $P_{\rm o} = 120$, 90, and 60 W when $v_{\rm in(rms)}$ varies from 198 to 242 V are sketched in Fig. 18(a) and (b), respectively. It can be seen from Fig. 18(a) that the efficiency of the proposed LED driver will increase along with the growth of input voltage or output power. The maximum efficiency can reach at around 88.7%. According to Fig. 18(b), the power factor will also increase along with the

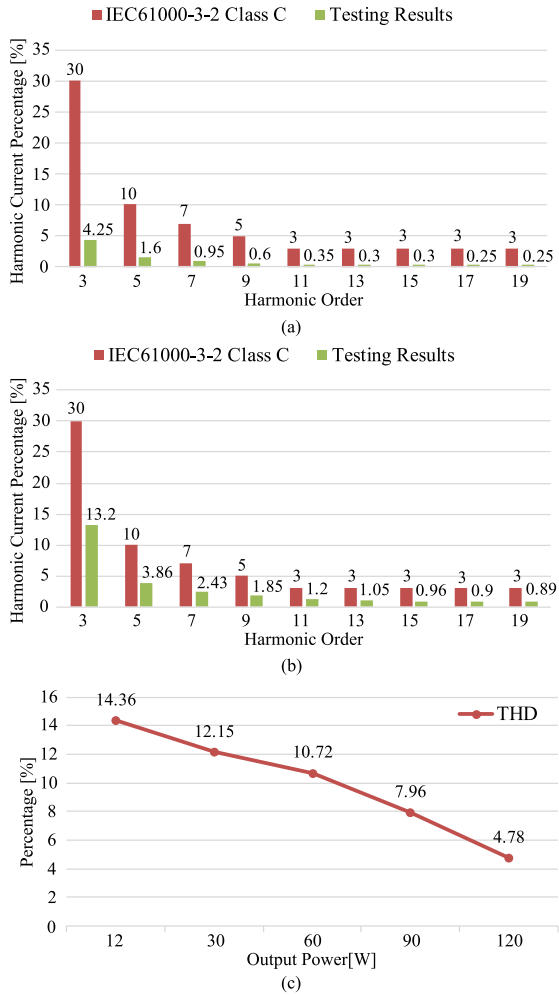

Fig. 19. THD testing results of the input current with $v_{\rm in(rms)} = 220$ V. (a) Input current harmonics percentage compared with IEC61000-3-2 Class C standard at $P_{\rm o} = 120$ W. (b) Input current harmonics percentage compared with IEC61000-3-2 Class C standard at $P_{\rm o} = 12$ W. (c) Measured THD with changing output power.

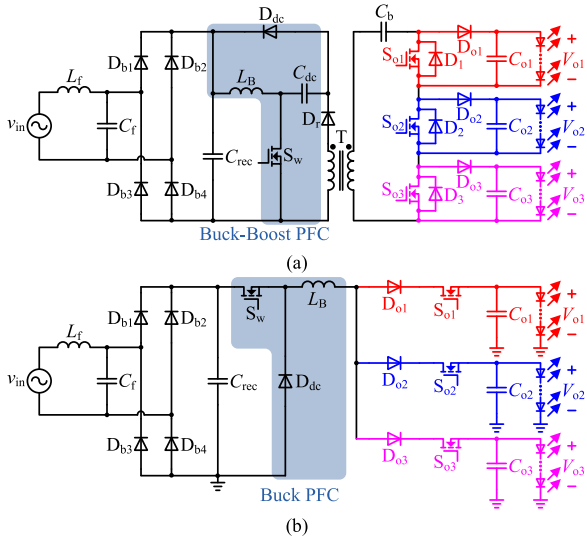

Fig. 20. Topologies of the series-type and parallel-type LED drivers. (a) Series-type LED driver in this paper. (b) Parallel-type LED driver presented in [18].

TABLE IV
COMPARATIVE ANALYSIS RESULTS BETWEEN THE LED DRIVERS IN THIS PAPER AND IN [18]

Items	The LED driver in this paper P_{total}=120 W			The LED driver presented in [18] P_{total}=120 W		
Input and output conditions	220 V, 0.5 A/0.7 A/1.0 A			220 V, 0.5 A/0.7 A/1.0 A		
Output structure	Series-type			Parallel-type		
AOUs can be driven concurrently	Yes			No		
Isolation	Yes			No		
PFC	Buck-Boost, DCM			Buck, DCM		
Current sampling	Isolated current sensor			Sampling resistor		
MOSFET gate drivers	Transformer-isolated gate driver / 4			High-side gate driver / 1 Low-side gate driver / 3		
Number of switches	4			4		
Number of diodes	5			4		
Electrolytic capacitor	1 (C_{dc})			3 (C_{o1}, C_{o2}, C_{o3})		
The value of inductor L_B	130 μH			15 μH		
The value of output filter capacitor	10 μF*2=20 μF			1000 μF		
Voltage stress of switching devices	S_w/D_{dc}	V_m+V_{dc}	454 V	S_w/D_{dc}	V_m	311 V
	D_r	$V_m+n(V_{Cb}-V_{o3})$	394 V	S_{o1}/D_{o1}	$0/(V_{o1}-V_{o3})$	0/40 V
	S_{o1}/D_{o1}	V_{o1}	80 V	S_{o2}	$(V_{o1}-V_{o2})$	23 V
	S_{o2}/D_{o2}	V_{o2}	57 V	D_{o2}	$(V_{o2}-V_{o3})$	17 V
	S_{o3}/D_{o3}	V_{o3}	40 V	S_{o3}/D_{o3}	$(V_{o1}-V_{o3})/0$	40 V/0
Current stress of switching devices	S_w	$\frac{V_m d_1 T_s}{L_B}+\frac{V_{dc} d_1 T_s}{L_m}+\frac{2I_{o3}}{nd_1}$	12.63 A	S_w/D_{dc}	$\frac{V_m - V_{o3}}{L_B} d_3 T_s$	16.93 A
	D_{dc}	$\frac{V_m d_1 T_s}{L_B}$	6.08 A	S_{o1}/D_{o1}	$\frac{V_m - V_{o1}}{L_B} d_1 T_s$	15.46 A
	D_r	$\frac{V_{dc} d_1 T_s}{L_m}+\frac{2I_{o3}}{nd_1}$	6.55 A			
	$S_{o1}/S_{o2}/S_{o3}$	$\frac{2I_{o3}}{d_1}$	7.87 A	S_{o2}/D_{o2}	$\frac{V_m - V_{o2}}{L_B} d_2 T_s$	16.23 A
	D_{o1}	I_{pk3}	2.55 A			
	D_{o2}	I_{pk2}	2.62 A	S_{o3}/D_{o3}	$\frac{V_m - V_{o3}}{L_B} d_3 T_s$	16.93 A
	D_{o3}	I_{pk2}	2.62 A			
Advantage	1. Electrical isolation can ensure safety 2. The current stresses of output-diodes are relatively small 3. The capacitances of output filter capacitors are relatively small 4. Fully independent control with zero cross-regulation			1. Non-isolation structure is relatively simple and modular 2. The voltage stresses of all switching devices are relatively small 3. The way of current sampling is simple which can reduce cost 4. Fully independent control with zero cross-regulation		
Disadvantage	1. The different AOU has different reference grounds 2. One more diode is used 3. Including electrolytic capacitor			1. The effective operating frequency of each LED channel is reduced 2. The current stresses of switches and diodes are relatively high 3. The capacitances of output filter capacitors are very large, so that electrolytic capacitors are also used		

growth of output power. The maximum power factor can reach 0.999.

In order to see the input current harmonics performance of the proposed series-type LED driver, the THD testing results of the input current with $v_{in(rms)} = 220$ V are shown in Fig. 19. The comparison results between the measured input current harmonics percentages and the IEC 61000-3-2 Class C standard at 120 W, 12 W are illustrated in Fig. 19(a) and (b), respectively. Clearly, the proposed series-type LED driver has lower input current harmonics contents and always can meet the corresponding maximum permissible harmonic current limits as defined by the IEC 61000-3-2 Class C standard. In addition, the measured THD with changing output power is also illustrated in Fig. 19(c). It can be seen that THD of the input current will be reduced remarkably along with the increasing of the output power and keeps lower than 15%.

VI. COMPARATIVE ANALYSIS

In this section, a detailed and fair comparative analysis has been made for the sake of further analyzing the different characteristics between the series-type LED driver proposed in this paper and the parallel-type one in [18]. For a clearer comparison, the topologies of the series-type and parallel-type LED drivers both have been depicted in Fig. 20(a) and (b) again as follows. Besides, all comparative results have been tabulated as shown in Table IV. Note that the ac input voltage, the total output power and three output currents of these two kinds of LED drivers above are all same here.

Compared with the topology structure of the parallel-type LED driver in [18], the most obvious difference of the proposed LED driver in this paper is the series-connected structure of all AOUs, which can ensure that all AOUs can be driven concurrently in a switching period. Naturally, the isolated current sensors and the isolated MOSFET gate drivers should be adopted due to the different reference grounds in the series-type output structure, to some extent, which will certainly increase some cost compared with the resistor sampling manner and low-side gate drivers in the parallel-type output structure. However, electrical isolation can be achieved in the proposed series-type LED driver for better security in some special occasions or high-power applications.

In another aspect, the proposed series-type LED driver has higher voltage stresses and lower current stresses of the switching devices, as shown in Table IV. By contrast, although the

voltage stresses of the switching devices in the parallel-type LED driver in [18] are relatively low, the current stresses of the switches and diodes are become higher since the inductance of $L_{\rm B}$ is relatively small, which seems to be more evident especially in the current stresses of $D_{\rm o1}$, $D_{\rm o2}$, and $D_{\rm o3}$. Thus, the low voltage and high current diode must be used, which will bring extra cost compared with the small-sized patch Schottky diodes used in the counterpart of the series-type LED driver in this paper. From this point of view, the parallel-type scheme presented in [18] is more suitable to be applied in low-power applications, while the series-type scheme in this paper will have more benefits along with the increasing of output power. Furthermore, the capacitances of three output filter capacitors in the parallel-type LED driver are very large since these three output filter capacitors have to perform the functions of energy storage and switching frequency filtering. Hence, these three output filter capacitors can only employ the electrolytic capacitors.

In conclusion, both the series-type output structure in this paper and the parallel-type output structure in [18] have their own different features, which are the two possible solutions to achieve fully independent control of N output currents without zero cross-regulation.

VII. Conclusion

This paper proposed a single-stage series-type LED driver with independent control of N-channel output currents according to the duality principle, which is another possible solution to achieve fully independent control of each output current compared with the parallel-type scheme. N AOUs are series-connected to form the series-type N-channel outputs structure, which makes it easier to regulate each output current independently by proposed ICCS. The experimental results indicate that fully independent control and zero cross-regulation of three output currents can be achieved as required, which have also demonstrated the effectiveness of the proposed series-type scheme and the correctness of parameter design method.

References

[1] B. Poorali and E. Adib, "Analysis of the integrated SEPIC-Flyback converter as a single-stage single-switch power-factor-correction LED driver," *IEEE Trans. Ind. Electron.*, vol. 63, no. 6, pp. 3562–3570, Jun. 2016.

[2] S. Wang, X. Ruan, K. Yao, S. C. Tan, Y. Yang, and Z. Ye, "A flicker-free electrolytic capacitor-less AC–DC LED driver," *IEEE Trans. Power Electron.*, vol. 27, no. 11, pp. 4540–4548, Nov. 2012.

[3] C. A. Cheng, C. H. Chang, T. Y. Chung, and F. L. Yang, "Design and implementation of a single-stage driver for supplying an LED street-lighting module with power factor corrections," *IEEE Trans. Power Electron.*, vol. 30, no. 2, pp. 956–966, Feb. 2015.

[4] J. He, X. Ruan, and L. Zhang, "Adaptive voltage control for bidirectional converter in flicker-free electrolytic capacitor-less AC–DC LED driver," *IEEE Trans. Ind. Electron.*, vol. 64, no. 1, pp. 320–324, Jan. 2017.

[5] K. Modepalli and L. Parsa, "A scalable N-Color LED driver using single inductor multiple current output topology," *IEEE Trans. Power Electron.*, vol. 31, no. 5, pp. 3773–3783, May 2016.

[6] S. K. Ng, K. H. Loo, Y. M. Lai, and C. K. Tse, "Color control system for RGB LED with application to light sources suffering from prolonged aging," *IEEE Trans. Ind. Electron.*, vol. 61, no. 4, pp. 1788–1798, Apr. 2014.

[7] X. Qu, S. C. Wong, and C. K. Tse, "Noncascading structure for electronic ballast design for multiple LED lamps with independent brightness control," *IEEE Trans. Power Electron.*, vol. 25, no. 2, pp. 331–340, Feb. 2010.

[8] H. Ma, J. S. Lai, Q. Feng, W. Yu, C. Zheng, and Z. Zhao, "A novel valley-fill SEPIC-derived power supply without electrolytic capacitor for LED lighting application," *IEEE Trans. Power Electron.*, vol. 27, no. 6, pp. 3057–3071, Jun. 2012.

[9] W. Chen and S. Y. R. Hui, "A dimmable light-emitting diode (LED) driver with Mag-Amp postregulators for multistring applications," *IEEE Trans. Power Electron.*, vol. 26, no. 6, pp. 1714–1722, Jun. 2011.

[10] H. J. Chiu, Y. K. Lo, J. T. Chen, S. J. Cheng, C. Y. Lin, and S. C. Mou, "A high-efficiency dimmable LED driver for low-power lighting applications," *IEEE Trans. Ind. Electron.*, vol. 57, no. 2, pp. 735–743, Feb. 2010.

[11] Y. Hu and M. M. Jovanovic, "LED driver with self-adaptive drive voltage," *IEEE Trans. Power Electron.*, vol. 23, no. 6, pp. 3116–3125, Nov. 2008.

[12] H. Chen, Y. Zhang, and D. Ma, "A SIMO parallel-string driver IC for dimmable LED backlighting with local bus voltage optimization and single time-shared regulation loop," *IEEE Trans. Power Electron.*, vol. 27, no. 1, pp. 452–462, Jan. 2012.

[13] S. Li, Y. Guo, S. C. Tan, and S. Y. Hui, "An off-line single-inductor multiple-output LED driver with high dimming precision and full dimming range," *IEEE Trans. Power Electron.*, vol. 32, no. 6, pp. 4716–4727, Jun. 2017.

[14] D. Ma, W. H. Ki, C. Y. Tsui, and P. K. T. Mok, "Single-inductor multiple-output switching converters with time-multiplexing control in discontinuous conduction mode," *IEEE J. Solid State Circuits*, vol. 38, no. 1, pp. 89–100, Jan. 2003.

[15] A. T. L. Lee, J. K. O. Sin, and P. C. H. Chan, "Scalability of quasi-hysteretic FSM-based digitally controlled single-inductor dual-string Buck LED driver to multiple strings," *IEEE Trans. Power Electron.*, vol. 29, no. 1, pp. 501–513, Jan. 2014.

[16] H. C. Kim, C. S. Yoon, H. Ju, D. K. Jeong, and J. Kim, "An AC-Powered, flicker-free, multi-channel LED driver with current-balancing SIMO buck topology for large area lighting applications," in *Proc. IEEE Appl. Power Electron. Conf. Expo.*, 2014, pp. 3337–3341.

[17] C. C. Chen, C. Y. Wu, Y. M. Chen, and T. F. Wu, "Sequential color LED back-light driving system for LCD panels," *IEEE Trans. Power Electron.*, vol. 22, no. 3, pp. 919–925, May 2007.

[18] Y. Guo, S. Li, A. T. L. Lee, S. C. Tan, C. K. Lee, and S. Y. R. Hui, "Single-Stage AC/DC single-inductor multiple-output LED drivers," *IEEE Trans. Power Electron.*, vol. 31, no. 8, pp. 5837–5850, Aug. 2016.

[19] X. Zhan, H. Chung, and R. Zhang, "Investigation into the use of single inductor for driving multiple series-connected LED channels," *IEEE Trans. Power Electron.*, vol. 32, no. 4, pp. 3034–3050, Apr. 2017.

[20] Y. C. Li and C. L. Chen, "A novel single-stage high-power-factor AC-to-DC LED driving circuit with leakage inductance energy recycling," *IEEE Trans. Ind. Electron.*, vol. 59, no. 2, pp. 793–802, Feb. 2012.

[21] Q. Luo, J. Huang, Q. He, K. Ma, and L. Zhou, "Analysis and design of a single-stage isolated AC-DC LED driver with a voltage doubler rectifier," *IEEE Trans. Ind. Electron.*, vol. 64, no. 7, pp. 5807–5817, Jul. 2017.

Jian Huang was born in Xichang, Sichuan Province, China, in 1989. He received the B.S. degree in electrical engineering from Southwest Petroleum University, Chengdu, Sichuan Province, in 2012. He is currently working toward the Ph.D. degree in electrical engineering from Chongqing University, Chongqing, China.

His research interests include LED drivers with multiple constant current outputs, dc voltage-/current-type distributed power systems and soft-switching techniques.

Quanming Luo (M'14) was born in Chongqing, China, in 1976. He received the B.S., M.S., and Ph.D. degrees in electrical engineering from Chongqing University, Chongqing, in 1999, 2002, and 2008, respectively.

He was the Research and Development Engineer with the Emerson Network Power Co. Ltd., Shenzhen, China, from 2002 to 2005. Since 2005, he has been working as a Professor with the College of Electrical Engineering, Chongqing University. He is the author or co-author of more than 40 papers in journal or conference proceedings. His research interests include LED driving systems, communication power systems, power harmonic suppression, and power conversion systems in electrical vehicles.

Qingqing He was born in Hubei Province, China, in 1993. She received the B.S. degree in electrical engineering from the Wuhan University of Technology, Hubei, China, in 2015. She is currently working toward the Ph.D. degree in electrical engineering from Chongqing University, Chongqing, China.

Her research interests include high-efficiency and high-reliability power converters and LED lighting systems.

Aqian Zu was born in Shaanxi Province, China, in 1994. She received the B.S. degree in electrical engineering from the Xi'an University of Technology, Shaanxi, China, in 2016. She is currently working toward the M.S. degree in electrical engineering from Chongqing University, Chongqing, China.

Her research interests include high-power LED drivers with constant current and power factor correction technology.

Luowei Zhou (M'04–SM'04) was born in Dujiangyan, China, in 1954. He received the B.S., M.S., and Ph.D. degrees in electrical engineering from Chongqing University, Chongqing, China, in 1982, 1988, and 2000, respectively.

Since 1982, he has been with the College of Electrical Engineering, Chongqing University, where he is currently a Full Professor. He was a Visiting Professor at the University of California, Irvine, CA, USA, between September 1998 and August 1999. He is the author or co-author of more than 70 papers. His research interests include the analysis and control of power electronics circuits, the realization of active power filters, power factor correction techniques, and high-frequency power conversion.

Prof. Zhou is the Vice-President of the China Society of Power Supply.